Results in Chemistry 4 (2022) 100475

Contents lists available at ScienceDirect

Results in Chemistry

journal homepage: www.sciencedirect.com/journal/results-in-chemistry

Investigation on crystallization kinetics using thermal analysis and crystalline behavior of yttrium iron garnet ($Y_3Fe_5O_{12}$) compounds

Jasper Goldwin [a,b], K. Aravinthan [b,c,1], J. Gajendiran [d,*], S. Gnanam [e], S. Gokul Raj [f,*], N. Karthick [f], G. Ramesh Kumar [g]

[a] Department of Physics, Agni College of Technology, Thalambur, Chennai 600130, India
[b] Bharathiyar University, Coimbatore 641046, India
[c] Department of Physics, Angel College of Engineering, Tiruppur 641665, India
[d] Department of Physics, Vel Tech Rangarajan Dr. Sagunthala R&D Institute of Science and Technology, Avadi, Chennai 600 062, India
[e] Department of Physics, School of Basic Sciences, Vels Institute of Science, Technology & Advanced Studies (VISTAS), Pallavaram, Chennai 600 117, India
[f] Department of Physics, C. Kandaswami Naidu College For Men (CKNC), (Affiliated to University of Madras, Chennai-600005, India) Annanagar, Chennai 600 102, India
[g] Department of Science and Humanities, University College of Engineering Arni-Thatchur-(Anna University, Chennai) 632 326, India

ARTICLE INFO

Keywords:
Nanocrystalline material
Thermal analysis
Structural properties

ABSTRACT

The objectives of this work were to investigate the crystallization kinetics of Yttrium Iron Garnet ($Y_3Fe_5O_{12}$, YIG) using the thermal analysis. The Differential Scanning Colorimetric (DSC) analysis confirmed that crystallization begins to form the YIG from the nitrates of the YIG gel product at the melting temperature of 337 °C. Two weight losses were discovered from the nitrates of the YIG gel product using simultaneous thermo gravimetric analysis (TGA) and differential thermal analysis (DTA), in the temperature range of 70 to 130 °C and 760 °C, indicating the amorphous state to change the crystalline state formation. A thermo magnetization analysis (TMA) was performed on the synthesized YIG calcined at 850 °C, and the Curie temperature results were thoroughly examined. The Williamson-Hall (W-H) plots and transmission electron microscope (TEM) analysis were used to study the crystalline strain and crystalline formation of the as-prepared YIG particles at 850 °C calcined temperatures.

1. Introduction

Many researchers have created rare earth iron garnet ($RE_3Fe_5O_{12}$) materials and studied their optical and magnetic behaviour in recent years, because the wide range of development introduced the above mentioned materials in optical communication systems, and microwave and magneto-optical based devices [1–8]. The choice of rare earth garnet material used in the above devices has been motivated by its high dielectric loss and excellent electromagnetic sensing behavior [9]. Among the rare earth garnets, Yttrium Iron Garnet (YIG) has received special attention in electro-optics-based device applications [6,10]. The position of cationic and anionic sites attached to the decahedral, octahedral, and tetrahedral sites forming a crystalline structure is determined by the optimization temperature of the YIG material synthesized [11]. Thermal analysis techniques such as TGA, DTA, DSC, and thermo-magnetization analysis have been used to identify the crystalline structure phase formation. The above-mentioned thermal analysis determined the crystallization kinetics behaviour, thermal stability, and optimization temperature of the YIG material's crystalline formation. We can synthesize single crystalline or polycrystalline (i.e.,crystalline orientation plane's alignment) YIG material with single or multiple phase structure, after identifying its thermal stability through a thermal analysis. As a result, the thermal analysis plays an important role in the development of YIG materials with crystalline formation.

The goal of this current work is to investigate the crystallization kinetics and Curie temperature of the synthesized Yttrium Iron Garnet ($Y_3Fe_5O_{12}$) material using thermal analysis techniques such as DSC, TGA, DTA, and TMA. Furthermore, the JMA equation has been used to explain the dimensional growth mechanisms of the garnet phase. In addition, the outcome of the crystalline strain characteristics and

* Corresponding authors.
E-mail addresses: gaja.nanotech@gmail.com (J. Gajendiran), sgokulraj@gmail.com (S. Gokul Raj).
[1] Currently in Department of Physics, PSG College of Arts & Science, Coimbatore 641014, India.

https://doi.org/10.1016/j.rechem.2022.100475
Received 9 June 2022; Accepted 6 August 2022
Available online 10 August 2022

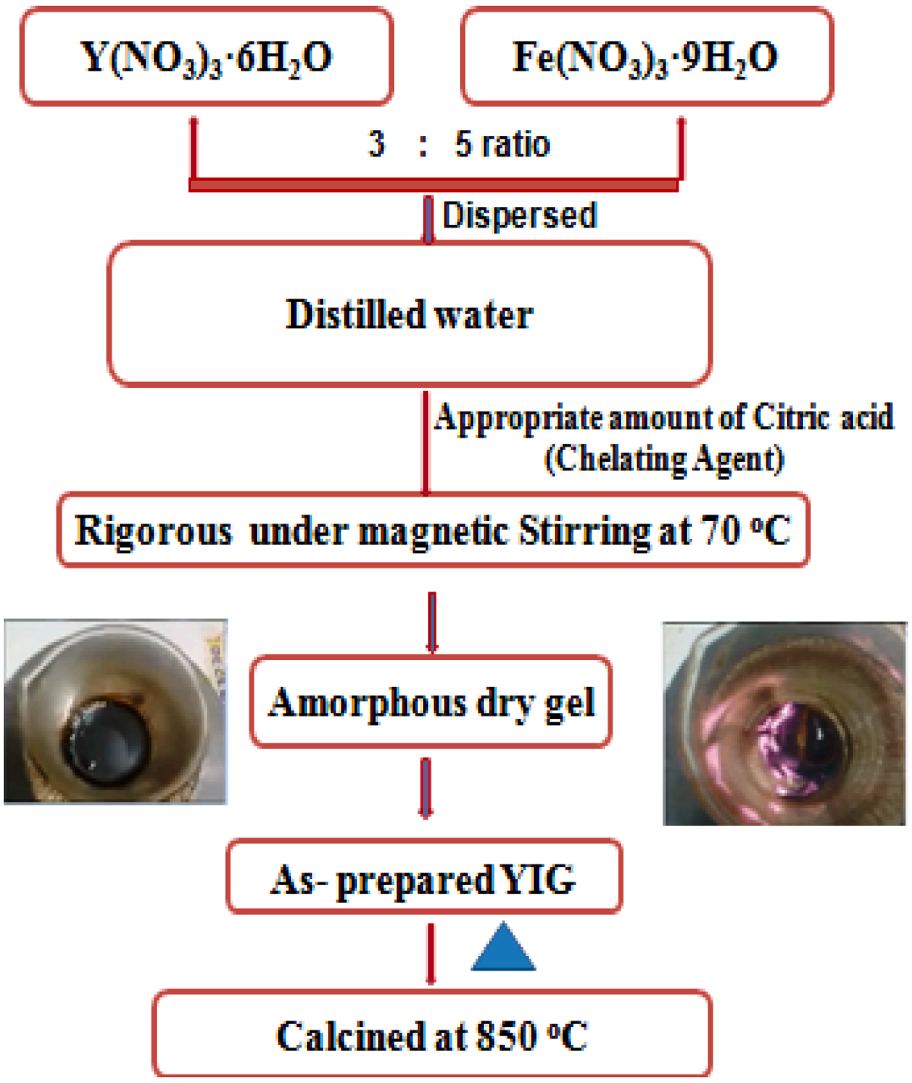

Fig. 1. Flowchart depicting the nanocrystalline formation of the YIG product via the sol–gel reaction step.

particle shape formation are discussed, using powder X-ray diffraction data made W-H plots and TEM studies from the YIG calcined at 850 °C.

2. Experimental

The experimental synthesis step of the nanocrystalline formation of the YIG product using rare earth metal nitrate precursor (yttrium nitrate hexahydrate), iron nitrate, and fuel (citric acid) in the presence of an aqueous medium via the sol gel reaction has been in detail in our previous report [12]. The detailed sol–gel reaction synthesis step is depicted in a flowchart shown in Fig. 1. The following thermal analyses, such as TGA, DSC, DTA, and Thermo Magnetization studies, were used to characterize the synthesis of the YIG gel product before the formation of nanostructured YIG powder [12]. Thermal analysis was performed on the gel nitrate of the yttrium garnet product in order to identify the crystallization formation of the YIG material.

The synthesized nitrates of the YIG gel product, as prepared YIG and the characterization of the YIG sample calcined at 850 °C and the corresponding instruments, specifications and results can be seen in Table 1.

3. Results and discussion

3. 1 Thermal analysis

A series of redox reactions is involved in the crystallization formation of YIG from nitrates of the YIG gel product. The thermal behavior (i.e. endothermic reaction) of the nitrates of the YIG gel product on increasing the temperature from 25 to 500 °C was recorded using DSC graphs and this is shown in Fig. 2. In the DSC curve, a single peak was detected at a temperature of 337 °C, indicating the nitrates of the YIG gel product's combustion temperature. In other words, 337 °C represents the melting temperature (T_m) of the endothermic reaction that produces the nitrates of the YIG gel. The YIG gel product was created using non-ionic surfactant 1, 2 ethane diol and when tested using DSC, it revealed a T_m value of 364 °C. In the current study, T_m (338 °C) was required, which is lower than that of the non-ionic surfactant assisted YIG gel product (T_m = 364 °C) [13].

The as-prepared YIG sample was heated using the TGA instrument at various heating rates such as 5, 10, 20, and 25 k/min, as shown in Fig. 3a. The TGA graphs revealed a loss of mass change of 16 % in temperatures ranging from 0 to 820 °C for the as-prepared YIG sample at various heating rates ranging from 5 to 25 K/min. The first weight loss occurred at temperatures ranging from 150 °C to 400 °C. This first weight loss is due to the loss of water molecules and organic residues,

Table 1

Characterizations	Instruments	Specifications	Important finding results
Powder XRD data	Rigaku Ultima III – X-ray diffractometer	CuK_{α} ($\lambda = 1.540$ Å) radiation, the diffraction pattern was scanned between ranges of 10 to 60°	Crystal structure, crystalline strain
DSC	NETZSCH STA 449F3 simultaneous analyzer	Nitrogen atmosphere at heating rate of 20 °C per minute from 30 °C to 400 °C	Thermal stability, Material phase formation
TG-DTA	Thermogravimetric analysis (TGA) was performed in a EXSTAR 6000 Thermogravimetric/ Differential Thermal Analyser (TG/DTA) equipment from ambient temperature to 1100 °C.	Nitrogen atmosphere at heating rate of 5, 10, 15, 20 and 25 Kper minute	Weight loss Thermal stability, Material phase formation
TMA	Thermomagnetic analysis was performed in the same equipment by placing a small permanent magnet beneath the sample in the temperature range from ambient to 350 °C.	–	Curie temperature
TEM	The morphology was examined using a JEOL EX-2000 Transmission electron microscope (TEM).	–	Particle shape formation

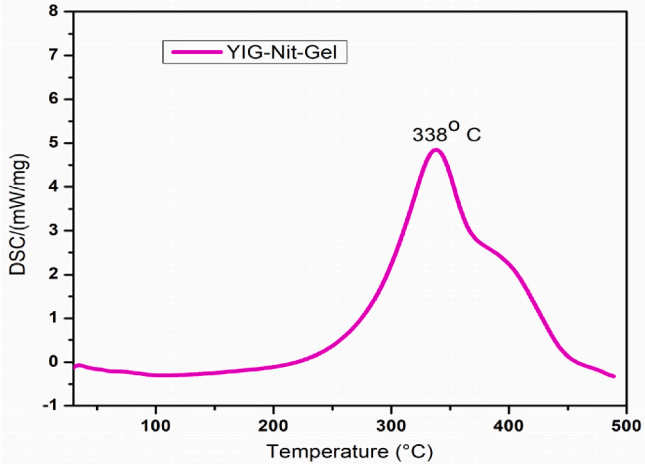

Fig. 2. DSC analysis of the YIG gel product.

indicating that the first phase transformation has occurred. The second stage phase transformation took place at temperatures ranging from 500 to 850 °C (second weight loss). The second weight loss demonstrates that crystallization began with the amorphous state transformation. In the TGA graphs, the weight loss shift was discovered under the influence of different heating rates for the prepared sample. Crystallization began on the prepared YIG sample at 765, 867, 827, 789 and 805 °C using the heating rates of 5 K/min, 10 K/min, 15 K/min, 20 K/min, and 25 K/min, respectively. Hence, the starting point of crystallization formation in the prepared YIG sample at a given temperature is determined by the

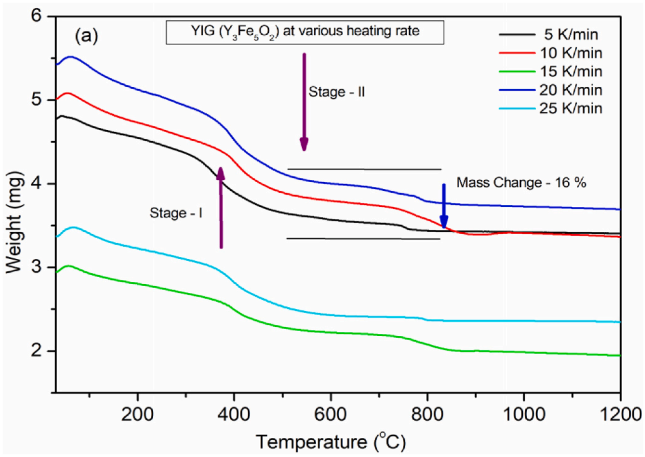

Fig. 3a. TGA of the as-prepared YIG sample.

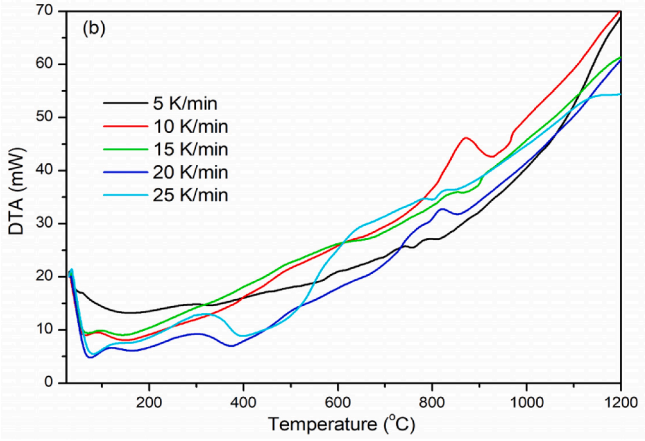

Fig. 3b. DTA of the as-prepared YIG sample at the heating rates of 5, 10, 20 and 25 K /min.

heating rate used in the TG instruments. When compared to other heating effect rates, the initial crystallization began from the amorphous state at 765 °C as the lower heating rate effect. As a result, the heating rate applied to the prepared samples plays an important role in the formation of the crystallization's starting point.

The DTA curve was recorded for the prepared YIG sample at heating rates of 5, 10, 20 and 25 K /min, with significant results shown in Fig. 3b. Only the weight loss above 760 °C for the as-prepared YIG sample at various heating rates of 5 to 25 K/min, as shown by the DTA curve (Fig. 3b), indicates true crystallization. Furthermore, only one stage crystallization occurred at all the heating rates.

Fig. 3c shows an enlarged view of the region between 300 and 500 °C. According to Fig. 3c, the crystallization temperature increased significantly as the heating rate increased from 5 K/min to 25 K/min. Fig. 3d shows an enlarged view of the region between 700 and 1000 °C. In addition, the graphs (Fig. 3b and c) show that as the heating rates increase, so does the first crystallization temperature (T). The crystallization temperature values are given in Table 2.

Thermo-magnetization was investigated for the YIG calcined at 850 °C and the results are shown in Fig. 4. The goal of the TG-MAG analysis for the YIG calcined at 850 °C was to determine the respective material phase transformation and its properties. The phase transformation occurred at a temperature of 272 °C, as shown by the TG-MAG graph. The temperature detected in the TG-MAG graph, indicates the Curie temperature. The experimentally determined Curie temperature of the YIG as calcined at 850 °C agrees well with the reported Curie

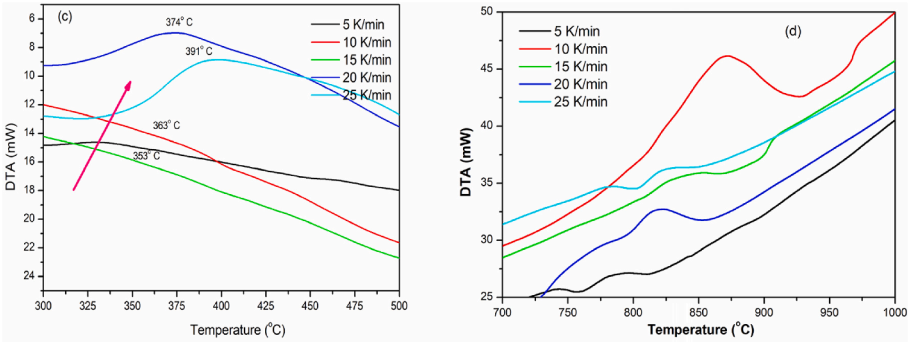

Fig. 3c and d. DTA of the as prepared YIG sample (c) enlarged view at temperatures between 300 and 500 °C and (d) enlarge view at temperatures between 700 and 1000 °C.

Table 2
Healing rate (β) vs crystallization temperature.

Sr.no	β	T
1	5	782
2	10	795
3	20	817
4	25	820

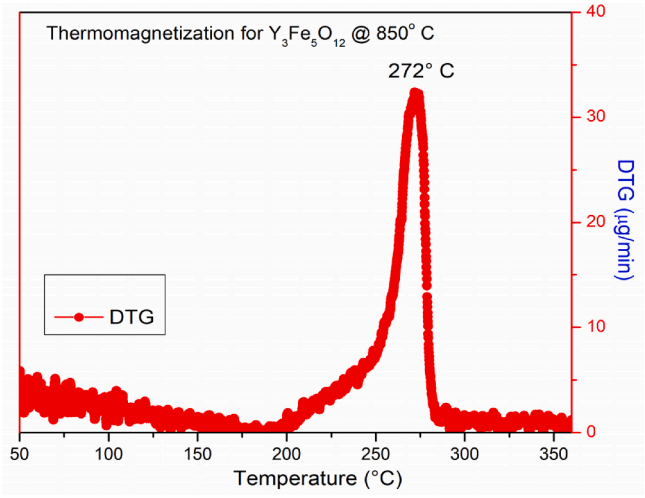

Fig. 4. Thermomagnetization curve of the YIG sample calcined at 850 °C.

temperature of the bulk and single crystal YIG compounds.

The values in Table 2 include one stage of crystallization. The activation energy for the crystallization of YIG was determined with the aid of the Johnson–Mehl–Avrami Kolmogorov (JMAK) equation, which is adopted from the Kissinger Plot.

The amount of crystallization that happened at any particular time is given by [14].

$$C(t) = 1 - \exp(-Kt)^n \quad (1)$$

where n – Avrami exponential component.

K – reaction rate constant.

The relation between the reaction rate (K), activation energy (E_a) and absolute temperature (T) can be connected through the Standard Arrhenius equation [14].

$$K = f_o e^{-E\alpha/RT} \quad (2)$$

where R- Universal gas Constant.

Using (1) and (2) correlate with each other to obtain the JAMK equation [14].

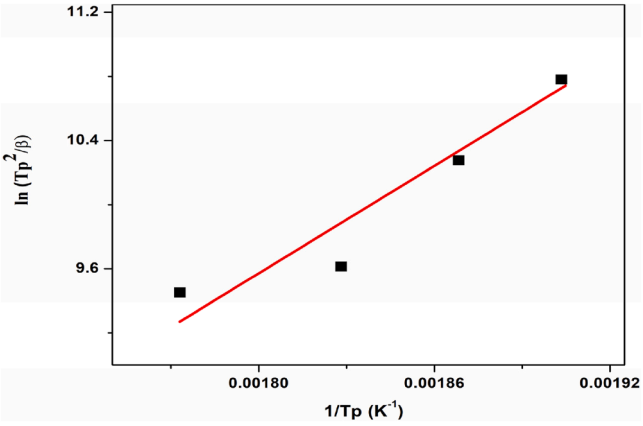

Fig. 5. $1/T_p$ vs ln (T_p^2/β) plot of as prepared YIG.

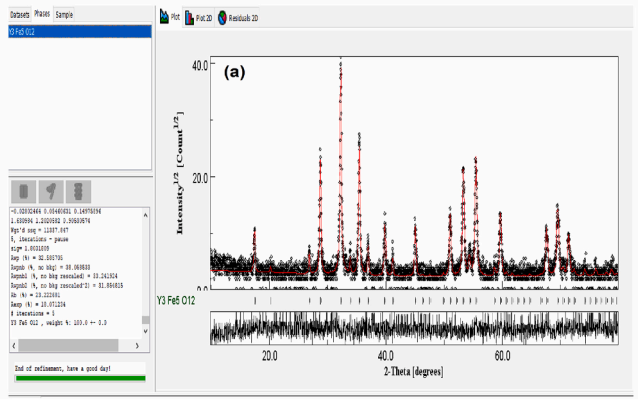

Fig. 6a. Maud fit analysis of the YIG calcined at 850 °C.

$$\ln\left(T_p^2/\beta\right) = \ln(E_a/R) - \ln V - E_a/RT \quad (3)$$

$1/T_p$ and ln (T_p^2/β) values are computed with the aid of the differential thermal analysis data at different heating rates of the as prepared YIG sample followed by $1/T_p$ on the x-axis and ln (T_p^2/β) on the y-axis plotted through the Gaussian fit. These are shown in Fig. 5. A straight line was detected from the $1/T_p$ vs ln (T_p^2/β). The slope and intercept values are detected from a straight line and its value substituted in the JMAK equation; the activation energy value of $Y_3Fe_5O_{12}$ was found to be 132 kJ/mol during crystallization.

Table 3
Diffraction angle (2θ) and FWHM values of YIG calcined at 850 °C.

	YIG sample calcined at 850 °C	
S.No.	2θ	FWHM
1	17.64493	0.16485
2	28.95252	0.17087
3	32.44767	0.18397
4	35.62709	0.18316
5	39.99003	0.1902
6	45.25007	0.1921
7	51.22898	0.24297
8	53.46993	0.25281
9	55.64384	0.27058
10	59.82941	0.26905
11	69.68987	0.34085
12	67.77947	0.30692

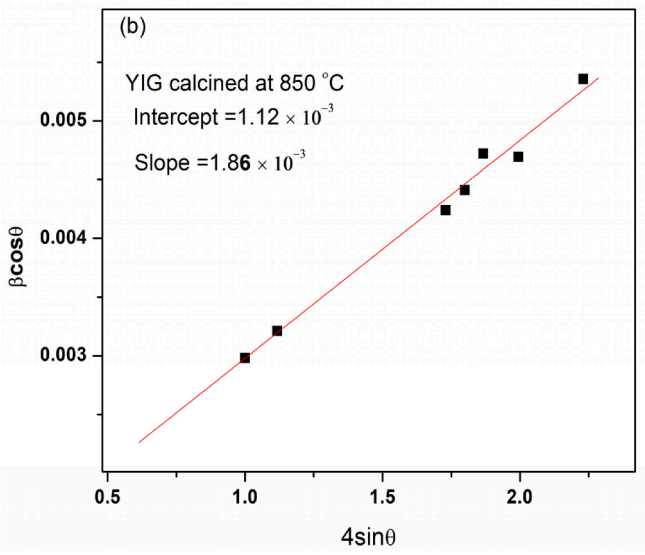

Fig. 6b. W-H plot of the YIG calcined at 850 °C.

3.2. MAUD fit and W-H plot analysis

The MAUD fit analysis (Fig. 6a) was performed on the YIG sample calcined at 850 °C in order to test the YIG phase and identify the compound. It can be concluded that the sample calcined at 850 °C confirmed the formation of the yttrium iron garnet material.

Powder XRD analysis was performed on the as-prepared and YIG samples calcined at 850 °C, and their crystalline phase, diffraction shift and size were examined in previous reports [12]. The purpose of this work was to investigate the crystalline strain value and other parameters using Gaussian linear fitting software and the extracted diffraction angles' (2θ) position and its corresponding Full Width Half Maximum (FWHM) values from the our previously reported powder XRD pattern of the YIG calcined at 850 °C samples [12].

The values of 2θ, and FWHM of the Bragg's peaks of the YIG sample calcined at 850 °C were derived from the powder XRD analysis and their values are presented in Table 3. The W-H plot for the YIG calculated at 850 °C was plotted by taking 2θ and FWHM values from Table 3 and is shown in Fig. 6b. The crystalline strain (ε) determined from the obtained W-H plot was 1.86×10^{-3}. In addition, the crystallite size was found to be 123 nm for the YIG sample calcined at 850 °C by substituting the intercept (Y) value of 1.12×10^{-3} using $D = K\lambda/y$.

Where, D-crystallite size, λ-X-ray wavelength (0.1540 nm), and y-intercept.

3.3. TEM analysis

The TEM image of the as-prepared YIG sample revealed highly aggregated spherical particles with dark images (as shown in Fig. 7). It was not possible to measure the size of the particles due to their dark and highly aggregated nature, whereas the TEM image of the YIG calcined at 850 °C revealed highly aggregated spherical particles with non-uniform sizes ~20–45 nm.

4. Conclusion

In this current work, the thermal analysis (DSC, TGA, DTA, and TMA) was used to investigate the melting temperature, weight loss, Curie temperature, and crystallization kinetics formation of synthesized nitrates of the YIG gel product, as-prepared YIG and calcined (850 °C) YIG sample. The kinetics of non-iso thermal crystallization as well as the dimensional growth mechanism of the garnet phase was also elucidated. Using powder X-ray diffraction data from a YIG sample calcined (850 °C), the full width half- maximum (FWHM) and diffraction angle position values were extracted, and the crystalline strain characteristics were derived using W-H plots. The crystalline strain value for the YIG sample calcined at 850 °C sample is 1.86×10^{-3} using a W-H plot. The particle shapes of the prepared YIG and that calcined at 850 °C were also explained using TEM studies. The thermal studies mentioned above would be very useful in determining the crystallization kinetics formation, and optimization temperature of any other metal ferrite and oxide of metal compounds.

CRediT authorship contribution statement

Jasper Goldwin: Methodology, Writing – original draft. **K. Aravinthan:** Writing – review & editing. **J. Gajendiran:** Investigation,

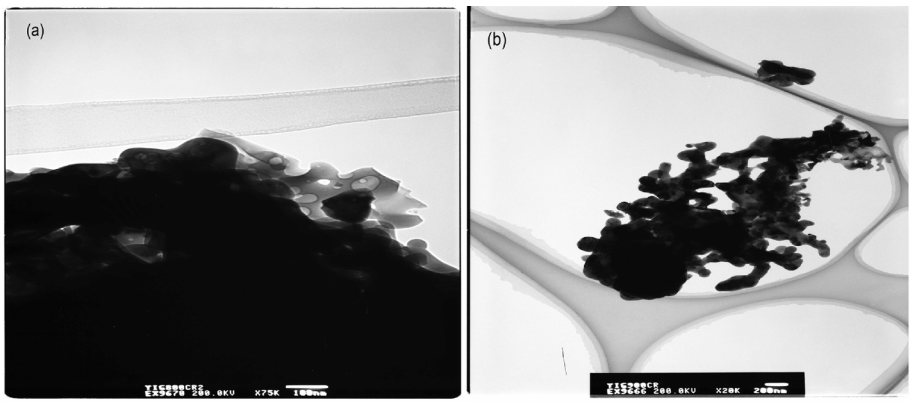

Fig. 7. TEM images of YIG (a) as-prepared and (b) calcined at 850 °C.

Writing – review & editing, Conceptualization. **S. Gnanam:** Writing – review & editing. **S. Gokul Raj:** Writing – review & editing. **N. Karthick:** Formal analysis. **G. Ramesh Kumar:** Writing – review & editing.

Declaration of Competing Interest

The authors declare that they have no known competing financial interests or personal relationships that could have appeared to influence the work reported in this paper.

Data availability

Data will be made available on request.

References

[1] Anjori Sharma, Sachin KumarGodara, A.K.Srivastava, Effect of Y^{3+}, Bi^{3+}, La^{3+} substitution on structural, optical and magnetic properties of gadolinium iron garnets, Mater. Tody Proceed. 50 (2022)1867-1877.

[2] M. Yousaf, A. Noor, S. Xu, M.N. Akhtar, B. Wang, Magnetic characteristics and optical band alignments of rare earth (Sm^{+3}, Nd^{+3}) doped garnet ferrite nanoparticles (NPs), Ceram. Int. 46 (10) (2020) 16524–16532.

[3] M. Norkus, A. Laurikenas, D. Vistorskaja, K. Mazeika, D. Baltrunas, RamunasSkaudzius, AldonaBeganskiene, Aivaras Kareiva, Investigation of substitution effects of the first four lanthanides (La, Ce, Pr and Nd) in yttrium iron garnet, J. Alloy. Compound 903 (2022) 16378.

[4] Ajay Kumar, RajeevKumar, Nancy Verma, A.V.Anupama, Harish, K.Choudhary, Reji Philip, Balaram Sahoo, Effect of the band gap and the defect states present within band gap on the non-linear optical absorption behaviour of yttrium aluminium iron garnets, Opt. Mater.108 (2020) 110163.

[5] A.N. Hapishah, M.N. Hamidon, M.M. Syazwan, F.N. Shafiee, Effect of grain size on microstructural and magnetic properties of holmium substituted yttrium iron garnets ($Y_{1.5}Ho_{1.5}Fe_5O_{12}$), Results Phys. 14 (2019), 102391.

[6] H. Li, Investigation of the structural, magnetic, impedance properties in samarium-doped yttrium iron garnet, Ceram. Int. 46 (10) (2020) 15408–15416.

[7] A. Raja, P.M. Mohammed Gazzali, G. Chandrasekaran, Enhanced electrical and ferrimagnetic properties of bismuth substituted yttrium iron garnets, Physica B Condensed Matter 613 (2021), 412988.

[8] M. Yang, H. Wang, T. Yang, B. Hu, H. Li, T. Li, Y. Zhou, H. Zhou, Y. Hu, H. Zhang, J. Zhao, Parallel-pumped nonlinear loss effects for polycrystalline yttrium iron garnet in the high-power microwave environment, Ceram. Int. 48 (8) (2022) 10952–10959.

[9] R. Fu, Y. Li, R. Peng, Y. Lu, Q. Wen, High dielectric constant yig ferrites with low sintering temperature, J. Mater. Sci. Electron. 33 (8) (2022) 4914–4923.

[10] Makiyyu Abdullahi Musa, Rabaah Syahidah Azis, Xiangting Dong, Nurul Huda Osman Jumiah Hassan, Farah Diana Muhammad, Nurhidayaty Mokhtar, Influence of aluminum substitution on microstructural, electrical, dielectric, and electromagnetic properties of sol-gel synthesized yttrium iron garnet (YIG), AIP Adv. 10 (2020) 045128.

[11] M. Akhtar, A. Bakar Sulong, M. Khan, M. Ahmad, G. Murtaza, M.R. Raza, R. Raza, M. Saleem, M. Kashif, Structural and magnetic properties of yttrium iron garnet (YIG) and yttrium aluminum iron garnet (YAIG) nanoferrites prepared by microemulsion method, J. Magn. Magn. Mater. 401 (2016) 425–431.

[12] J. Goldwin, K. Aravinthan, S. Gokul Raj, G.R. Kumar, Synthesis and characterization of yttrium iron garnet ($Y_3Fe_5O_{12}$) magnetoelectric applications, Digest J. Nanomater. Biostruct. 14 (2019) 721–725.

[13] O. Opuchovic, A. Kareiva, K. Mazeik, D. Baltrun, Magnetic nanosized rare earth iron garnets $R_3Fe_5O_{12}$:Sol-gel fabrication, characterization and reinspection, J. Magn. Magn. Mater. 422 (2017) 425–433.

[14] M. Manonmani, V. Jaikumar, S. Gokul Raj, G. Ramesh Kumar, Crystallization, non-isothermal kinetics and structural analysis of nanocrystalline multiferroic bismuth ferrite ($BiFeO_3$) synthesized by combustion method, J. Thermal Anal. Calorimetry 138 (1) (2019) 185–193.